

Statistical properties of the localization measure of chaotic eigenstates in the Dicke modelQian Wang^{2,1} and Marko Robnik¹¹*CAMTP-Center for Applied Mathematics and Theoretical Physics, University of Maribor, Mladinska 3, SI-2000 Maribor, Slovenia*²*Department of Physics, Zhejiang Normal University, Jinhua 321004, China*

(Received 15 July 2020; accepted 25 August 2020; published 10 September 2020)

The quantum localization is one of the remarkable phenomena in the studies of quantum chaos and plays an important role in various contexts. Thus, an understanding of the properties of quantum localization is essential. In spite of much effort dedicated to investigating the manifestations of localization in the time-dependent systems, the features of localization in time-independent systems are still less explored, particularly in quantum systems which correspond to the classical systems with smooth Hamiltonian. In this work, we present such a study for a quantum many-body system, namely, the Dicke model. The classical counterpart of the Dicke model is given by a smooth Hamiltonian with two degrees of freedom. We examine the signatures of localization in its chaotic eigenstates. We show that the entropy localization measure, which is defined in terms of the information entropy of Husimi distribution, behaves linearly with the participation number, a measure of the degree of localization of a quantum state. We further demonstrate that the localization measure probability distribution is well described by the β distribution. We also find that the averaged localization measure is linearly related to the level repulsion exponent, a widely used quantity to characterize the localization in chaotic eigenstates. Our findings extend the previous results in billiards to the quantum many-body system with classical counterpart described by a smooth Hamiltonian, and they indicate that the properties of localized chaotic eigenstates are universal.

DOI: [10.1103/PhysRevE.102.032212](https://doi.org/10.1103/PhysRevE.102.032212)**I. INTRODUCTION**

Quantum chaos studies the features of quantum systems with a classical chaotic counterpart. Several remarkable features of chaos in a wide variety of quantum systems have been revealed, including the level statistics of energy spectra [1–6], hypersensitivity to perturbation [7–9], and the exponential increase of the out-of-time-order correlator [10,11]. As an important concept in quantum physics, quantum chaos is a very active research field during the last and present century. In particular, in the past few decades, both the experimental and theoretical progresses (see Ref. [12] for review) in the study of quantum many-body systems have triggered a great deal of efforts upon understanding chaos in quantum open systems [13–16] and quantum many-body systems [17–20], as well as its impacts on the non-equilibrium processes, such as quantum thermalization and equilibration (see, for example, the reviews [21,22]).

One of the major progresses in the studies of quantum chaos is the discovery of the quantum localization (or dynamical localization) in the dynamics of systems with time-periodic perturbations [23–26]. This effect is a quantum suppression of classical chaotic diffusion due to the destruction of quantum interference, and closely related to the well-known Anderson localization in one-dimensional disordered systems [27]. It was first unveiled in the quantum kicked-rotator [26,28], and later studied in many other systems [29–31], particularly in quantum many-body systems in recent years [32–34].

At the same time, investigating the characterization of quantum localization in conservative systems has also attracted some attention [35–37]. Based on the Wigner band random matrix model [38], the features of quantum localization in conservative systems have been studied through the global structure of eigenstates and an explicit connection between localization and level repulsion exponent was established [36]. However, as details of real quantum systems cannot be captured by the standard random matrix theory, the features of quantum localization in time-independent systems, therefore, still require more explorations. It is worth pointing out that the quantum localization of the conservative systems is related to the dynamical localization in the kicked-rotator and therefore to the Anderson localization, but is nevertheless quite different [26,28,37].

Recently, an analysis of quantum localizations in different billiards by means of Husimi function has been done in several works [39–44]. One remarkable property of quantum localization that has been revealed in these studies is the probability distribution of the localization measure has a universal form, which is in good agreement with the so called β distribution. Furthermore, it has been found that the level repulsion exponent shows a linear dependence on the averaged localization measure. In the present work, we continue and extend these works to a quantum many-body system. In contrast to billiards, the classical counterpart of the system studied in this work is given by a smooth Hamiltonian with two degrees of freedom. Specifically, we explore the properties of quantum localization in the Dicke model.

Dicke model describes the interaction between a set of identical two-level atoms and a single electromagnetic mode within a cavity [45]. As a prototypical spin-boson model, the Dicke model has been widely employed in different contexts, such as quantum phase transitions [46–51], nonequilibrium dynamics [52–54], thermalization [55,56], the scrambling process [57,58], quantum batteries [59], and quantum chaos [60–65]. The recent experimental realizations of the Dicke model in ultracold atoms [66–68] and ion traps [69] have renewed further interest in studying the Dicke model.

In this work, we present a detailed investigation of the localization of chaotic eigenstates of the model. Following the method outlined in Refs. [43,44], we will consider the statistical properties of the entropy localization measure defined in terms of the information entropy of Husimi distribution for chaotic eigenstates. We show that the localization measure and the normalized participation number are linearly related and, therefore, equivalent. Moreover, we also find that the localization measure probability distribution can be well described by the so called β distribution, as in the results observed in billiards. As shown in the different billiards, the dependence between the level repulsion exponent and the averaged localization measure in our study is still given by a linear function. Therefore, we believe that all statistical properties of the localized chaotic eigenstates revealed in our work are universal, independent of the specific studied system.

The rest of the article is organized as follows. In Sec. II, we introduce the Dicke model together with its classical counterpart and discuss the known transition from integrability to chaos using the level statistics and Poincaré sections in quantum and classical cases, respectively. We also identify the parameter and energy regimes considered in this work via the chaotic fraction in this section. In Sec. III we show how to calculate the Husimi function of individual eigenstates, analyze the localization condition in chaotic eigenstates, explain how to separate the regular and chaotic eigenstates, define the entropy localization measure, and demonstrate that it is

equivalent to the participation number. We then provide the detailed numerical studies of the distribution of localization measures in different parameter regimes and discuss the connection between the level repulsion exponent and the averaged localization measure in Sec. IV. Finally, we summarize our results and give an outlook on the future perspectives in Sec. V.

II. DICKE MODEL AND ITS CLASSICAL LIMIT

A. Dicke model

In this work, we consider the Dicke model [45], which describes an ensemble of N two-level atoms with level spacing ω_0 coupled with a single cavity mode with frequency ω and has been studied in many different fields of physics. By setting $\hbar = 1$ (throughout this work), the Hamiltonian of Dicke model reads

$$H = \omega a^\dagger a + \omega_0 J_z + \frac{2\kappa}{\sqrt{N}} J_x (a^\dagger + a), \quad (1)$$

where a^\dagger (a) is the bosonic creation (annihilation) operator, κ is the atom-field coupling strength, and J_x, J_y, J_z are the collective pseudospin operators and satisfy the SU(2) algebra.

The Hamiltonian in Eq. (1) commutes with the total spin operator $[H, \mathbf{J}^2] = 0$ with $\mathbf{J}^2 = J_x^2 + J_y^2 + J_z^2$. Therefore, one can divide the Hamiltonian matrix into totally independent diagonal blocks in \mathbf{J}^2 . In our study, we restrict ourselves to the maximum spin sector $j = N/2$, which includes the ground state. Moreover, as the parity operator $\Pi = e^{i\pi(a^\dagger a + J_z + j)}$ also commutes with H , the Hamiltonian matrix can be further separated into even- and odd-parity blocks. In the following, only the even-parity spectrum of the model will be considered.

We consider the basis set $\{|n; j, m_z\rangle = |n\rangle \otimes |j, m_z\rangle\}$ of the Hilbert space. Here, $|n\rangle$ with $n = 0, 1, \dots, \infty$ being the eigenstates of bosonic mode, while $|j, m_z\rangle$ with $m_z = -j, \dots, j$ are the so-called Dicke states of atomic sector. Then, the elements of the Hamiltonian matrix in this basis are given by

$$\begin{aligned} \langle n'; j, m'_z | H | n; j, m_z \rangle &= (n\omega + m_z\omega_0) \delta_{n',n} \delta_{m'_z,m_z} + \frac{\kappa}{\sqrt{N}} [\sqrt{n} \delta_{n',n-1} + \sqrt{n+1} \delta_{n',n+1}] \\ &\times [\sqrt{j(j+1) - m_z(m_z-1)} \delta_{m'_z,m_z-1} + \sqrt{j(j+1) - m_z(m_z+1)} \delta_{m'_z,m_z+1}]. \end{aligned} \quad (2)$$

Note that the system has infinite number of bosons, the dimension of the Hamiltonian matrix is therefore infinite. To numerically diagonalize its Hamiltonian, we must truncate the bosonic Hilbert space at a larger but finite dimension \mathcal{N}_c , which guarantees the convergence of the solution. In our study, the bosonic basis was truncated at $\mathcal{N}_c = 320$, the stability of the obtained results against the variation of \mathcal{N}_c has been carefully checked.

It is well known that the Dicke model shows very rich interesting features, such as the transition from the normal phase to superradiant phase in both thermal and quantum cases [46,47], and the excited-state quantum phase transitions in its energy spectra [48–52]. In particular, it has been found that for finite but sufficiently large N the Dicke

model exhibits a crossover from integrability to quantum chaos as the coupling strength passes through the critical value $\kappa_c = \sqrt{\omega_0\omega}/2$, where the dramatic changes in the nearest-neighbor-level spacing distribution $P(s)$ occur, where s denotes the level spacing between two consecutive unfolded energy levels [46,47,57]. Specifically, when $\kappa < \kappa_c$, $P(s)$ is approximately given by the Poisson distribution, i.e., $P(s) = e^{-s}$. For $\kappa > \kappa_c$, however, the level repulsion in the energy spectrum leads to $P(s)$ following the Wigner-Dyson distribution, $P(s) = (\pi/2)s \exp(-\pi s^2/4)$. The behaviors of $P(s)$ for different values of κ are shown in panels (a)-(d) of Fig. 1. Clearly, $P(s)$ exhibits a transition from Poisson distribution to Wigner-Dyson distribution as κ increases.

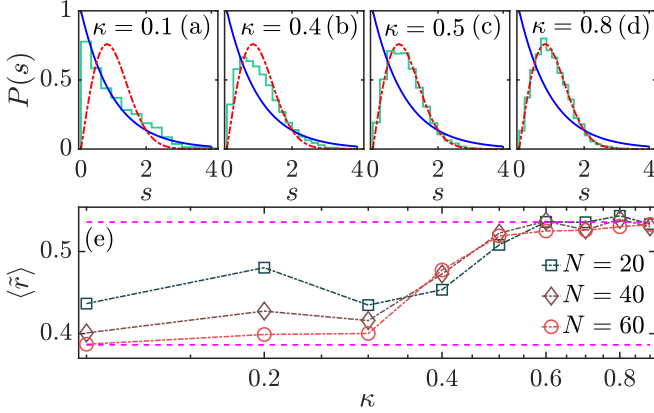


FIG. 1. (a–d) Distribution of neighbor-level spacing $P(s)$ in Dicke model for several control parameters κ with $N = 60$. The red dotted-dashed and blue solid curves in each panel show the Wigner-Dyson and Poisson distributions. (e) Averaged $\langle \tilde{r} \rangle$ as a function of κ for different system sizes. The two dashed lines denote $\langle \tilde{r} \rangle_W = 4 - 2\sqrt{3} \approx 0.536$ (upper) and $\langle \tilde{r} \rangle_P = 2 \ln 2 - 1 \approx 0.386$ (bottom), respectively. The other parameters are: $\omega = \omega_0 = 1$. All quantities are dimensionless.

To further illustrate the transition from regularity to chaos in Dicke model, we consider the ratio of consecutive level spacing \tilde{r} defined as [70]

$$\tilde{r}_n = \min\left(\delta_n, \frac{1}{\delta_n}\right), \quad (3)$$

where $\delta_n = s_n/s_{n-1}$ with $s_n = E_n - E_{n-1}$ is the nearest-neighbor spacing for a set of energy levels $\{E_n\}_{n=1}^N$ in ascending order. Because the distribution of \tilde{r} is independent of the local density of states, it has attracted lots of attention in recent years in the studies of quantum many-body chaos [71–76]. In particular, the average of \tilde{r}_n over energy levels, denoted by $\langle \tilde{r} \rangle$, has been used as a useful discriminator for different statistics of the energy-level-spacing distributions. It is known that $\langle \tilde{r} \rangle_P = 2 \ln 2 - 1 \approx 0.386$ for the Poisson-level spacing, while $\langle \tilde{r} \rangle_W = 4 - 2\sqrt{3} \approx 0.536$ for Gaussian orthogonal ensemble (GOE) [70,71].

Figure 1(e) plots $\langle \tilde{r} \rangle$ as a function of κ for several system sizes. We can see that $\langle \tilde{r} \rangle$ shows a transition from close to Poisson value $\langle \tilde{r} \rangle_P$ to the finally GOE value $\langle \tilde{r} \rangle_W$ with an increase in κ . We can further identify that the departures from the Poisson and GOE values of $\langle \tilde{r} \rangle$ at small and greater κ are only the finite size effect. By increasing the system size, we observe that $\langle \tilde{r} \rangle$ tends to the expected Poisson and GOE values at low and high values of κ , respectively. The value of $\langle \tilde{r} \rangle$ changing from Poisson value to GOE value is in agreement with the behaviors of the nearest-level spacing distribution $P(s)$ [cf. Fig. 1(a)–1(d)]. We finally notice that the abrupt change in $\langle \tilde{r} \rangle$ is approximately located in the region $\kappa \in [0.3, 0.6]$, which includes the critical value $\kappa_c = 0.5$.

B. Classical limit of the Dicke model

The classical counterpart of Eq. (1) can be obtained by using the normalized coherent states representation for the bosonic and pseudospin sectors, respectively [60]. The definition of the bosonic and pseudospin coherent states are

given by [77]

$$|\alpha\rangle = e^{-\alpha a^\dagger/2} e^{\alpha a^\dagger} |0\rangle, \\ |\mu\rangle = (1 + \mu\mu^*)^{-j} e^{\mu J_+} |j, -j\rangle. \quad (4)$$

Here, $\alpha, \mu \in \mathbb{C}$, $|0\rangle$ is the bosonic field vacuum state, and $|j, -j\rangle$ being the ground state of the atoms. By employing the relations

$$\langle \alpha | a | \alpha \rangle = \alpha, \quad \langle \alpha | a^\dagger | \alpha \rangle = \alpha^*, \\ \langle \mu | J_z | \mu \rangle = -j \left(\frac{1 - |\mu|^2}{1 + |\mu|^2} \right), \\ \langle \mu | J_x | \mu \rangle = j \left(\frac{\mu + \mu^*}{1 + |\mu|^2} \right), \quad (5)$$

one can find the expectation value of Hamiltonian Eq. (1) in the coherent state, given as

$$\mathcal{H}(\alpha, \mu) = \omega |\alpha|^2 - \omega_0 j \left(\frac{1 - |\mu|^2}{1 + |\mu|^2} \right) \\ + \frac{\kappa \sqrt{2j}}{1 + |\mu|^2} (\mu + \mu^*) (\alpha + \alpha^*). \quad (6)$$

To express \mathcal{H} in terms of the classical canonical variables, as was done in Refs. [60,61], we transform the original coherent parameters (μ^*, μ) and (α^*, α) to the canonical coordinates (q_1, p_1) and (q_2, p_2) according to the following transformation:

$$\mu = \frac{p_1 + iq_1}{\sqrt{1 - (p_1^2 + q_1^2)}}, \quad \alpha = \sqrt{\frac{4j}{2}} (p_2 + iq_2). \quad (7)$$

Here, (q_1, p_1) are the canonical variables in the atomic sector and related to the angular momentum J_x, J_y by $q_1/p_1 = J_y/J_x$, while (q_2, p_2) are the usual coordinates in the classical phase space of the field sector. Substituting Eq. (7) into Eq. (6), after some algebra, one can find the rescaled classical Hamiltonian in the following form [60,61]:

$$\mathcal{H}_{cl}(q_1, p_1, q_2, p_2) = \frac{\mathcal{H}}{4j} = \frac{\omega_0}{2} (p_1^2 + q_1^2) + \frac{\omega}{2} (p_2^2 + q_2^2) \\ + 2\kappa p_1 p_2 \sqrt{1 - (p_1^2 + q_1^2)} - \frac{\omega_0}{4}. \quad (8)$$

The classical equations of motion are, therefore, given by

$$\dot{q}_1 = \omega_0 p_1 + 2\kappa p_2 \sqrt{1 - (p_1^2 + q_1^2)} - \frac{2\kappa p_2 p_1^2}{\sqrt{1 - (p_1^2 + q_1^2)}}, \\ \dot{p}_1 = -\omega_0 q_1 + \frac{2\kappa p_1 p_2 q_1}{\sqrt{1 - (p_1^2 + q_1^2)}}, \\ \dot{q}_2 = \omega p_2 + 2\kappa p_1 \sqrt{1 - (p_1^2 + q_1^2)}, \quad \dot{p}_2 = -\omega q_2. \quad (9)$$

The above discussed quantum chaotic behavior is associated with the classical chaos in Eq. (9). To visualize the classical regular and chaotic behavior as a function of the coupling parameter in the classical system, we investigate the dynamics of the classical system as a function of the coupling parameter κ , employing the Poincaré sections, to get a qualitative insight of the crossover between regularity

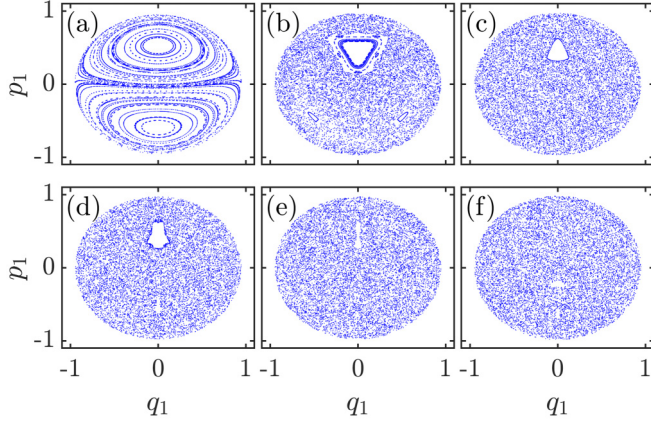


FIG. 2. Classical Poincaré section for (a) $\kappa = 0.1$, (b) $\kappa = 0.4$, (c) $\kappa = 0.46$, (d) $\kappa = 0.5$, (e) $\kappa = 0.54$, and (f) $\kappa = 0.7$, with fixed rescaled energy $\epsilon = E/j = 0.8$ and $\omega = \omega_0 = 1$. All quantities are dimensionless.

and chaos. In our study, for a fixed energy E , the Poincaré section is defined by the intersection of the classical trajectories with the surface $q_2 = 0$, with p_2 being fixed by the energy conservation for a given rescaled energy $\epsilon = E/j$, $\mathcal{H}_{cl}(q_1, p_1, q_2 = 0, p_2) = \epsilon/4$, which results in two values of p_2 :

$$p_2^\pm = -\frac{2\kappa}{\omega} p_1 \sqrt{1 - p_1^2 - q_1^2} \pm \sqrt{\frac{4\kappa^2}{\omega^2} p_1^2 (1 - p_1^2 - q_1^2) + \left[\frac{\omega_0 + \epsilon}{2\omega} - \frac{\omega_0}{\omega} (p_1^2 + q_1^2) \right]}.$$

Moreover, only the traversals with $p_2 > 0$ are recorded. Poincaré sections for several values of κ with $\omega_0 = \omega = 1$ and $\epsilon = 0.8$, are shown in Fig. 2.

We observe that at small κ [Fig. 2(a)], the Poincaré section consists of the regular orbits. Increasing the value of κ , a number of chaotic orbits emerge and the Poincaré sections exhibit the mixed feature with the regular regions coexisting with the chaotic regions [see Figs. 2(b)–2(e)]. When the value of κ is further increased, the whole phase space is covered by the chaotic orbits, as is evident from Fig. 2(f).

C. Chaotic fraction in classical phase space

To quantify the mixed structure of Poincaré sections exemplified in Fig. 2, we divide the whole phase space into the regular parts which are occupied by the regular trajectories, and the chaotic parts which are filled with chaotic trajectories. Then, for the phase space with fixed energy E , we define the chaotic fraction f_c as [39]

$$f_c = \frac{\Phi_c}{\Phi_t} = \frac{\int d\mathbf{q}d\mathbf{p} \chi_c \delta[H(\mathbf{q}, \mathbf{p}) - E]}{\int d\mathbf{q}d\mathbf{p} \delta[H(\mathbf{q}, \mathbf{p}) - E]}. \quad (10)$$

Here, Φ_t is the volume of the energy surface $H(\mathbf{q}, \mathbf{p}) = E$ in the entire phase space, Φ_c is the volume of the chaotic components, and χ_c denotes the characteristic function with $\chi_c = 1$ for chaotic components and $\chi_c = 0$ for other components. The

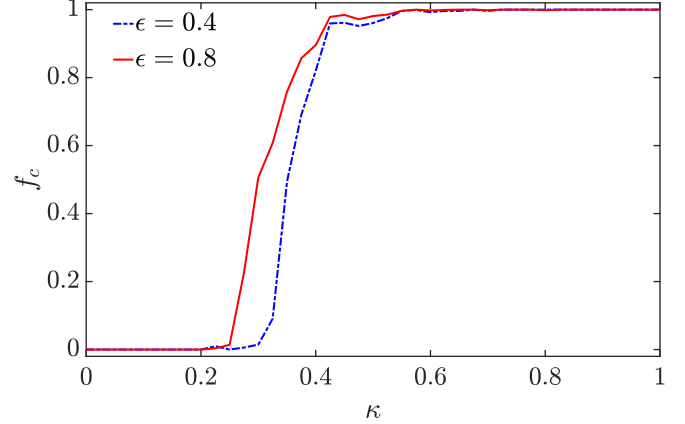


FIG. 3. Chaotic fraction f_c of the classical phase space as a function of κ with $\omega = \omega_0 = 1$ for different rescaled energies $\epsilon = E/j$. All quantities are dimensionless.

chaotic fraction f_c measures the overall degree of chaos and, therefore, takes values between 0 for fully regular dynamics and 1 when the system is dominated by the completely chaotic dynamics.

By employing the method outlined in Ref. [39], we have numerically investigated the chaotic fraction f_c as a function of κ with ϵ is fixed. The dependence of the chaotic fraction f_c on the coupling strength κ is shown in Fig. 3 for two values of the rescaled energy in resonant $\omega = \omega_0 = 1$ case. The chaotic fraction f_c exhibits a similar behavior as a function of κ for different energies. Namely, for small κ the regularity (almost integrability) of the system implies that the chaotic fraction is zero and keeps zero value up to a certain coupling strength κ_u , from which it increases with κ , approaching the saturation value $f_c = 1$ at $\kappa \sim 0.6$. A remarkable feature in Fig. 3 is that f_c shows a strongly energy-dependent property when $0 < f_c < 1$. This means that the degree of chaos in Dicke model also depends on the energy of the system. Indeed, as shown in Refs. [57,62–65], the chaotic degree of Dicke model depends not only on the coupling parameter κ but also on the energy of the system, unlike the billiard systems where the chaotic fraction f_c is independent of the energy. Note that the behavior of f_c is in agreement with the behavior of the Poincaré sections shown in Fig. 2.

The chaotic fraction f_c as a function of κ and energy $\epsilon = E/j$ is plotted in Fig. 4(a). A very complex nonmonotonous behavior of f_c can be clearly observed. The system is regular for small κ and ϵ , while the regularity of the system is decreased with increasing κ and/or ϵ . To study the localization properties of energy eigenstates, we will focus on the energy region with f_c fixed at f_c^s that fulfill $0 < f_c^s < 1$ for several values of control parameter κ . The horizontal and vertical cuts in Fig. 4(a) with different ϵ and κ , respectively, are plotted in Figs. 4(b) and 4(c). We find that the chaotic fraction f_c is fixed at $f_c^s = 0.965 \pm 0.003$ for $\kappa \in (0.44, 0.53)$ and $\epsilon \in (0.44, 0.95)$ [see the gray regions in Figs. 4(b) and 4(c)]. In the following of our study, we will reveal the localization properties of the chaotic eigenstates with energy located in the above mentioned regions with the control parameter κ varying between 0.44 and 0.53.

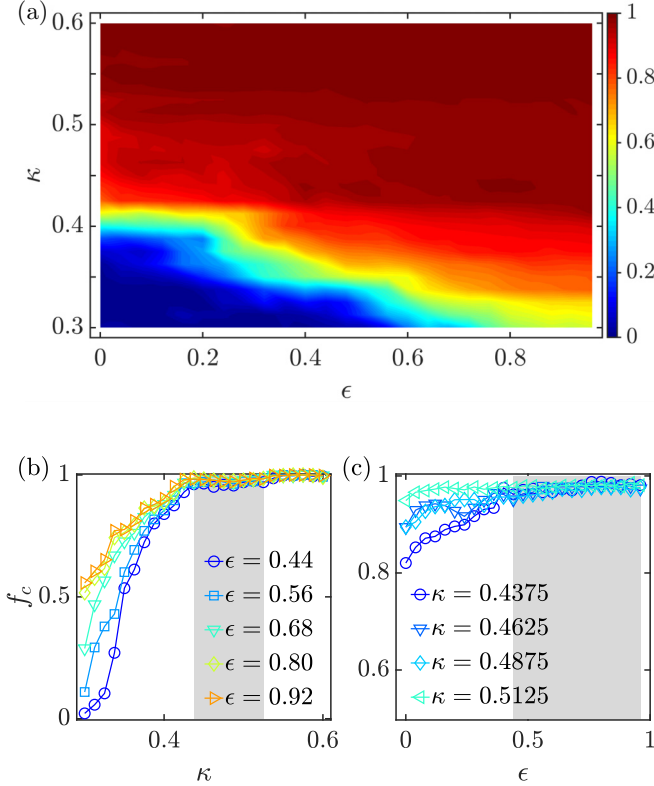


FIG. 4. (a) Heat map plotting the chaotic fraction f_c of the classical phase space as a function of κ and $\epsilon = E/j$. (b) f_c as a function of κ for different energies $\epsilon = E/j$. The gray region corresponds to the control parameters satisfy $\kappa \in (0.43, 0.53)$. (c) f_c as a function of $\epsilon = E/j$ for several values of κ . The gray region denotes $\epsilon \in (0.44, 0.95)$. The other parameters are: $\omega = \omega_0 = 1$. The axes in all figures are dimensionless.

III. HUSIMI FUNCTION AND THE LOCALIZATION OF CHAOTIC EIGENSTATES

While the above utilized quantities, i.e., $P(s)$ and $\langle \tilde{r} \rangle$, are useful to explore the quantum chaos, they can only be used for energy intervals. In the present work, we aim to identify the localization features in individual energy eigenstates, by employing the Husimi function which allows us to measure the degree of chaos for each energy eigenstate. We will use the Husimi functions to reveal the localization properties of the eigenstates that exhibit classically chaotic dynamics. It is worth pointing out that studying the quasiprobability distribution of the quantum eigenstates in classical phase space allows us to get more insights into the properties of the eigenstates and the relations between the quantum system and its classical correspondent [78].

A. Husimi function

As one of the simplest quasiprobability distributions in the phase space, the Husimi function provides a powerful tool to study the quantum-classical correspondence in quantum systems. The Husimi function can be considered as the Gaussian smoothed Wigner function [79] and defined as the projection of the wave function onto the minimal uncertainty (coherent) state [80]. For the k th energy eigenstate $|E_k\rangle$ of the Dicke

model, the Husimi function is given by

$$H_k(\alpha, \mu) = |\langle \alpha, \mu | E_k \rangle|^2, \quad (11)$$

where $|\alpha, \mu\rangle = |\alpha\rangle \otimes |\mu\rangle$ is the product coherent state with coherent states $|\alpha\rangle$ and $|\mu\rangle$ given in Eq. (4). The Dicke model has two degrees of freedom, the Husimi function $H_k(\alpha, \mu)$ is, therefore, defined in the four-dimensional phase space and is normalized as [81,82]

$$\int_{\mathbb{R}^4} H_k(\alpha, \mu) dz(\alpha, \mu) = 1. \quad (12)$$

Here, the integration measure reads

$$dz(\alpha, \mu) = \frac{2j+1}{\pi^2(1+|\mu|^2)^2} d^2\alpha d^2\mu, \quad (13)$$

with $d^2v = d\text{Re}(v)d\text{Im}(v)$ ($v = \alpha, \mu$).

The Husimi function in Dicke model has been used to explore the thermalization [55,56], quantum phase transition [81,82], quantum-classical correspondence [83,84], as well as the quantum chaos [62,63,85]. In addition, we note that the zeros of the Husimi function for energy eigenstates can precisely uncover the underlying classical dynamics [85]. Moreover, we would like to point out that the participation number calculated from the Husimi function has been established as a useful tool to identify the quantum chaos in the Dicke model [62,63].

To better visualize the Husimi function, and be able to compare with the classical calculations, as was done in Refs. [84,85], we study the spin Husimi function [83], which is obtained by projecting the Husimi function $H_k(\alpha, \mu)$ into the phase space of the atomic sector [84,85]

$$H_k(\mu) = \int \frac{d^2\alpha}{\pi} H_k(\alpha, \mu). \quad (14)$$

In our study, the Hamiltonian Eq. (1) is diagonalized in the Dicke basis $|nm\rangle = |n\rangle \otimes |m\rangle$ with $|n\rangle$ and $|m\rangle$ being the eigenstates of $a^\dagger a$ and J_z , respectively. Thus, the k th energy eigenstate $|E_k\rangle$ of the system can be written as

$$|E_k\rangle = \sum_{n=0}^{\infty} \sum_{m=-j}^j C_{nm}^k |nm\rangle, \quad (15)$$

where C_{nm}^k are the expanding coefficients and satisfy the normalization condition $\sum_{nm} |C_{nm}^k|^2 = 1$. Then the spin Husimi function in Eq. (14) can be explicitly computed as [84,85]

$$H_k(\mu) = \sum_{nml} C_{nm}^{k*} C_{nl}^k \langle \mu | l \rangle \langle m | \mu \rangle. \quad (16)$$

Numerically, we calculate the above Husimi function on the grid points (r, θ) with $0 \leq r \leq 1$, $-\pi \leq \theta < \pi$ in the phase space of atomic sector. Here, the polar coordinates have been employed to describe the phase space of atomic sector according to

$$q_1 = r \cos \theta, \quad p_1 = r \sin \theta.$$

Throughout this work, the grid of 250×250 points has been utilized.

In Fig. 5, we plot the spin Husimi functions of the energy eigenstates in an energy region around $E_0/j = 0.8$ for different values of κ . We first observe the remarkable change in the

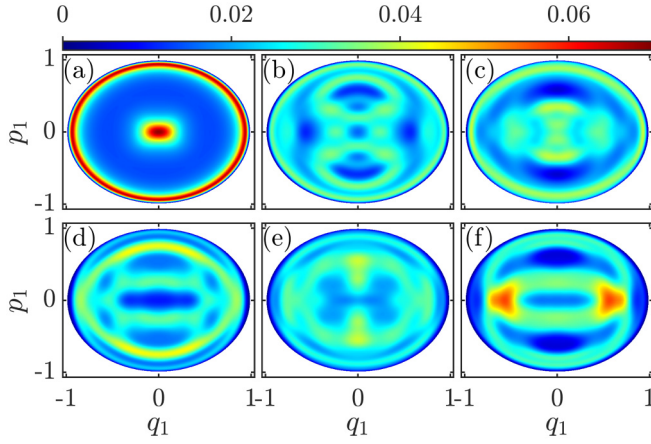


FIG. 5. Spin Husimi function $H_k(\mu)$ for (a) $\kappa = 0.1, k = 346, E_k/j = 0.8031$, (b) $\kappa = 0.4, k = 388, E_k/j = 0.8014$, (c) $\kappa = 0.46, k = 402, E_k/j = 0.8004$, (d) $\kappa = 0.5, k = 414, E_k/j = 0.8004$, (e) $\kappa = 0.54, k = 426, E_k/j = 0.8008$, and (f) $\kappa = 0.7, k = 482, E_k/j = 0.8004$. The other parameters are: $N = 40$ and $\omega = \omega_0 = 1$. The axes in all figures are dimensionless.

feature of spin Husimi functions when κ is varied. Specifically, the spin Husimi function concentrates in the phase space

$$\frac{\omega}{2j}\rho(\epsilon) = \begin{cases} \frac{1}{\pi} \int_{\eta_-}^{\eta_+} \arccos \sqrt{\frac{2\kappa_c^2(\eta - \epsilon)}{\kappa^2(1 - \eta^2)}} d\eta, & \epsilon_m \leq \epsilon < -1, \\ \frac{\epsilon + 1}{2} + \frac{1}{\pi} \int_{\epsilon}^{\eta_+} \arccos \sqrt{\frac{2\kappa_c^2(\eta - \epsilon)}{\kappa^2(1 - \eta^2)}} d\eta, & -1 \leq \epsilon \leq 1, \\ 1, & \epsilon > 1. \end{cases} \quad (18)$$

Here, $\eta_{\pm} = -\kappa_c^2/\kappa^2 \pm \kappa_c\sqrt{2(\epsilon - \epsilon_m)}/\kappa$ and $2\epsilon_m = -(\kappa_c^2/\kappa^2 + \kappa^2/\kappa_c^2)$. In Fig. 6(a), we plot t_H as a function of κ for several values of the system size N . For the parameter region studied in this work one can see that the Heisenberg time t_H grows linearly with κ , and it also increases with the rescaled energy ϵ , as shown in Fig. 6(b). Since the density of states in Eq. (18) depends linearly on the system size, the larger is the system size N , the greater is the Heisenberg time, as expected.

For the classical diffusion time t_D , as was done in Refs. [41,42], we identify t_D as the time at which an ensemble of initial conditions that are uniformly distributed in the momentum space at $p = 0$ with zero variance attains a certain fraction of the saturation value. The degree of chaos has strong impacts on the diffusion process in the classical systems, thus, the dependence of f_c on ϵ and κ indicates that the value of t_D will strongly depend on the coupling strength and the energy of the system. We illustrate the dependence of the classical diffusion time t_D on the coupling strength κ for different rescaled energies in Fig. 6(c). In our numerical calculation, t_D is defined by the time at which the variance of the momentum distribution reaches its asymptotic value, see the inset in Fig. 6(c) for the case with $\kappa = 0.4733, \epsilon = 0.8$. Clearly,

when κ is small, while it extends over the whole phase space for greater κ . By comparing to the classical Poincaré section illustrated in Fig. 2, we find that the extension of the spin Husimi function in classical phase space allows us to analyze the degree of chaos in each energy eigenstate. In this work we go further to explore the localization property in the chaotic energy eigenstates by employing the spin Husimi function.

B. Localization in the chaotic eigenstates

As shown in Refs. [40–42], the localization phenomenon in the eigenstates is determined by the ratio, denoted by α , between the Heisenberg time t_H and the classical diffusion time t_D ,

$$\alpha = \frac{t_H}{t_D}. \quad (17)$$

It is known that $\alpha \gg 1$ corresponds to the semiclassical condition, for which the chaotic eigenstates are delocalized for the systems that have the classical chaotic counterpart. The localization in the eigenstates occurs when $\alpha \leq 1$, which can appear also in the chaotic states in the mixed-type systems with $0 < f_c < 1$.

The Heisenberg time t_H is calculated as $t_H = 2\pi\rho(E)$, where the density of states of the Dicke model $\rho(E)$ is given by [49]

the classical diffusion time t_D decreases with κ and converges toward a constant at larger values of κ . This is consistent with the fact that the degree of chaos increases with increasing the coupling strength κ . Moreover, because the larger rescaled energy ϵ means the higher degree of chaos, we would expect that t_D decreases with ϵ for fixed κ . In particular, t_D will approach a constant value at higher values of ϵ , regardless of the coupling strength. The numerical results in Fig. 6(d) fully confirm these predictions.

Let us turn our attention to the behavior of α . The Heisenberg time t_H scales linearly with κ , while the classical diffusion time t_D decreases with increasing coupling strength κ . One, therefore, can expect that the time ratio α will increase with κ . In Fig. 7(a), we plot α as a function of the coupling strength κ for system sizes ranging from $N = 40$ to $N = 56$ with $\epsilon = 0.5$. It can be seen that α increases with increasing κ and it becomes greater than 1 when $\kappa \geq 0.5$, regardless of the system size. For different system sizes, since t_H is sensitive to N , we find that the value of α is strongly dependent on the system size N , the larger is N , the greater is the value of α . The variations of α with rescaled energy ϵ for different system sizes with fixed κ behave in a similar way, as seen in Fig. 7(b).

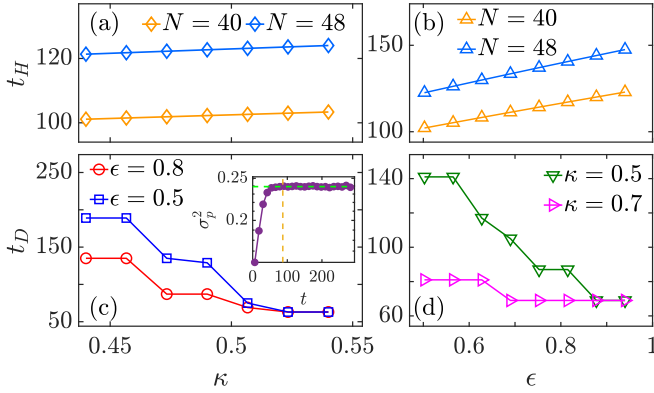


FIG. 6. (a) Heisenberg time t_H versus the coupling strength κ in the Dicke model for several system sizes with $\epsilon = 0.5$ and $\omega = \omega_0 = 1$. (b) t_H as a function of ϵ for different system sizes with $\kappa = 0.48$ and $\omega = \omega_0 = 1$. (c) Classical diffusion time t_D against the coupling strength κ for different rescaled energies ϵ with $\omega = \omega_0 = 1$. The inset shows the variance of momentum $\sigma_p^2 = \langle p^2 \rangle - \langle p \rangle^2$ vs. t for $\kappa = 0.4733$ with $\epsilon = 0.8$. Here, σ_p^2 is calculated with 4000 initial conditions that are uniformly distributed in the chaotic region with $q_0 \in [-0.8, 0.8]$ and $p_0 = 0$. The green dashed horizontal line indicates the long time averaged value of σ_p^2 , while the orange dashed vertical line denotes the time t_D at which σ_p^2 reaches its long time averaged value. (d) t_D as a function of ϵ for different coupling strengths with $\omega = \omega_0 = 1$. The axes in all figures are dimensionless.

C. Separation of chaotic and regular eigenstates

For the purpose to analyze the properties of the localized chaotic eigenstates, it is necessary to separate the chaotic eigenstates from the regular ones. To this end, as was done in Refs. [6,41,43], we label each point on the grid by an index $\Upsilon_{r,\theta}$. We set $\Upsilon_{r,\theta} = +1$ when the grid point belongs to the classical chaotic regions and $\Upsilon_{r,\theta} = -1$ if the grid point lies in the classical regular regions. Then, we take an initial condition in the chaotic region and evolve it according to the classical equations of motion in Eq. (9) until $\tau_f = 10^5$, which is enough for convergence. The value of $\Upsilon_{r,\theta}$ for each visited cell (r, θ)

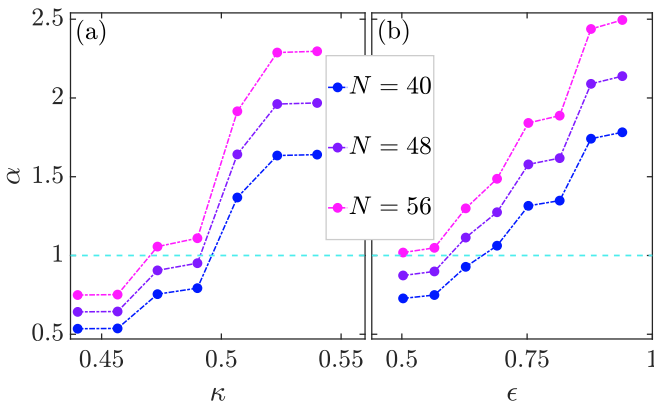


FIG. 7. (a) $\alpha = t_H/t_D$ as a function of κ for several system sizes N with $\epsilon = 0.5$. (b) α as a function of the rescaled energy $\epsilon = E/j$ for different system sizes N with $\kappa = 0.5$. The dashed horizontal lines in both panels indicate $\alpha = 1$. The other parameters are: $\omega = \omega_0 = 1$. All quantities are dimensionless.

on the grid is, therefore, given by $+1$, while $\Upsilon_{r,\theta} = -1$ for the remaining cells. The overlap between Husimi function $H_k(r, \theta)$ and indexes $\Upsilon_{r,\theta}$ on the grid is quantified by M_k defined as

$$M_k = \int dS \Upsilon_{r,\theta} H_k(r, \theta), \quad (19)$$

where dS is the normalized area form in the phase space of atomic sector.

In principle, M_k should be either $+1$ or -1 ; however, due to the reasons pointed out in Refs. [41,43], the actual value of M_k varies from -1 to $+1$. Hence, we need to find the threshold value M_t , such that all chaotic states are identified by $M_k \geq M_t$ and those associated with $M_k < M_t$ are regular. Two natural criteria have been used to decide the value of M_t , quantum and classical criterions [6,41]. In our study, as we want to ensure that only the chaotic eigenstates have been used, we have taken $M_t = 0.5$.

D. Localization measure of the chaotic eigenstates

The degree of localization of the chaotic eigenstates is quantified by the entropy localization measure A , defined in terms of the normalized information entropy of the Husimi distribution. For the k th eigenstate, the localization measure A_k is, in general [42,43],

$$A_k = \frac{\exp(\mathcal{I}_k)}{\mathcal{N}_{pc}}, \quad (20)$$

where for f degrees of freedom we have $\mathcal{I}_k = -\int dV H_k(p, q) \ln[(2\pi\hbar)^f H_k(p, q)]$ with dV being the volume form in the classical phase space. Here, $\mathcal{N}_{pc} = \Phi_c / (2\pi\hbar)^f$ is the number of the Planck cells in the chaotic region with Φ_c being the the volume of the classically chaotic region. Clearly, if the normalized Husimi function is supported by a single Planck cell, i.e., $H_k = 1 / (2\pi\hbar)^f$, then $\mathcal{I}_k \equiv 0$ and $A_k = 1 / \mathcal{N}_{pc} \approx 0$, which means the strongest localization. However, if H_k is uniform over the entire region Φ_c , then we have $\mathcal{I}_k = 1 / \Phi_c$, and therefore $A_k \equiv 1$, which is the complete extendedness (delocalization).

In our specific case, the considered atomic sector phase space with $f = 1$, by using the dimensionless quantities and performing the normalization, the localization measure can be rewritten as

$$A_k = \frac{\exp(I_k)}{\Omega_c}, \quad (21)$$

where Ω_c is the the phase space area of the chaotic component and $I_k = -\int dS H_k(r, \theta) \ln[H_k(r, \theta)]$ with dS being the normalized area form in the atomic sector phase space. A_k in Eq. (21) is defined in the interval $A_k \in [0, 1]$ with $A_k = 0$ corresponding to the maximally localized states and $A_k = 1$ for the fully delocalized states.

As is well known, to measure the degree of localization in a quantum state, the most widely used quantity is the participation number P_R [62,63,86–90]. By expanding a pure quantum state $|\Psi\rangle$ in a basis $|\nu_k\rangle$ with dimension \mathcal{N}_d , P_R is defined as

$$P_R = \frac{1}{\sum_{k=1}^{\mathcal{N}_d} |\langle \nu_k | \Psi \rangle|^4}. \quad (22)$$

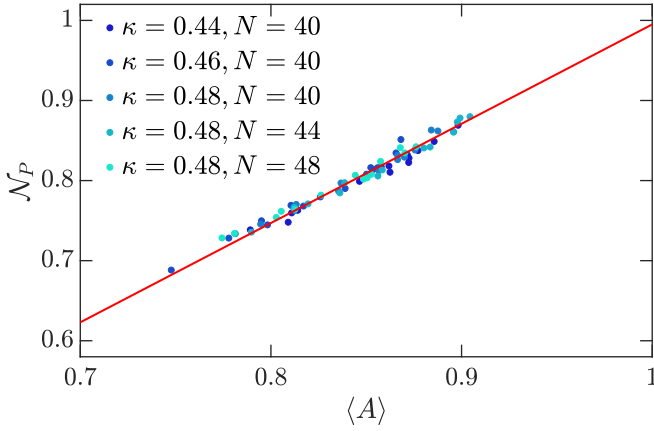


FIG. 8. Normalized participation number \mathcal{N}_p , defined in Eq. (23), as a function of A for several coupling strengths and system sizes with $\omega = \omega_0 = 1$. There are fitted by a linear function $y = 1.24x - 0.42$ (indicated by the red solid line), thus equivalent. The chaotic states that we have used in our calculation are the states with $M_k \geq M_t = 0.5$. The axes in the figure are dimensionless.

In the case of the maximum localization $P_R = 1$, while the strongest delocalization corresponds to $P_R = \mathcal{N}_d$ [62]. Participation number has been employed to characterize the localization-delocalization transitions in various studies. In particular, for the Dicke model, it has been used to study the regularity-chaos transition [62,63] and the equilibration process [91,92].

Therefore, one can pose the question as to whether there exists connection between A_k studied in this work and the participation number. To address this question, for the k th eigenstate, we consider the normalized participation number \mathcal{N}_p with the following expression:

$$\mathcal{N}_p = \frac{1}{\Omega_c} \frac{1}{\int dSH_k^2(r, \theta)}. \quad (23)$$

In Fig. 8, we plot \mathcal{N}_p as a function of A for different values of system size and coupling strength. Note that due to the fluctuation in localization measures, the results have been averaged over 20 eigenstates. As we can see, numerical data for different N and κ exhibit a good collapse and are fitted by a linear function $\mathcal{N}_p \propto A$, which means that A is equivalent to \mathcal{N}_p . We should mention that the equivalence between A and \mathcal{N}_p has also been verified in quantum billiard systems [43]. Hence, our result further confirms that the linear dependence between A and \mathcal{N}_p is a general conclusion, independent of the specific system. In our study, we take A as the measure of localization and focus on the statistical properties of A .

IV. STATISTICAL PROPERTIES OF THE ENTROPY LOCALIZATION MEASURE

Below we explore the properties of localization measure in terms of its probability distribution $P(A)$ and the relationship between the localization measure and the level repulsion exponent. Recent works for different billiards have revealed that the localization measure probability distribution is described by the β distribution and the level repulsion exponent is a linear function of the averaged localization measure [42,43]. We

expect that these results still hold in our study, even if we are dealing with a more complicated quantum many-body system with classical counterpart given by the smooth Hamiltonian.

We evaluate A for the chaotic eigenstates with energy in the range $\epsilon \in (0.44, 0.95)$ (see Sec. II C) for several coupling strengths κ . For each case, the chaotic states are identified according to the method given in Sec. III C with $M_t = 0.5$.

A. Localization measure probability distribution

We consider the localization measure operator defined as

$$\hat{\mathcal{A}} = \frac{\exp(\hat{\mathcal{I}})}{\Omega_c}, \quad (24)$$

where $\hat{\mathcal{I}} = -\int dS \hat{\mathcal{P}}_{r,\theta} \ln \hat{\mathcal{P}}_{r,\theta}$, with $\hat{\mathcal{P}}_{r,\theta} = |\mu\rangle\langle\mu| = |r, \theta\rangle\langle r, \theta|$. Then, we construct the projector onto the subspace with a given value of A and write it as

$$\delta(\hat{\mathcal{A}} - A) = \frac{1}{2\pi} \int_{-\infty}^{\infty} d\xi e^{i\xi(\hat{\mathcal{A}} - A)}, \quad (25)$$

where the integral representation of the delta function has been employed. The localization measure probability distribution is, therefore, given by the expectation value of this projector,

$$P(A) = \langle \delta(\hat{\mathcal{A}} - A) \rangle, \quad (26)$$

where $\langle \cdot \rangle$ denotes the expectation value with respect to the chaotic eigenstates of the system. Its Fourier transform representation (characteristic function) can be written as

$$P(A) = \frac{1}{2\pi} \int_{-\infty}^{\infty} d\xi \mathcal{X}(\xi) e^{-i\xi A}, \quad (27)$$

where $\mathcal{X}(\xi) = \text{Tr}(\rho_k^a e^{i\xi \hat{\mathcal{A}}})$ is the characteristic function of $P(A)$ with ρ_k^a being the reduced density matrix of the atomic sector. The fully localized state gives $\mathcal{X}(\xi) = 1$ and, therefore, $P(A) = \delta(A)$. The other extreme of the maximally delocalized state implies $\mathcal{X}_p(\xi) = e^{i\xi}$ and we would have $P(A) = \delta(A - 1)$, as expected.

In our numerical simulation, the spin Husimi function in Eq. (14) of the k th chaotic eigenstate is calculated on the grid in the phase space of atomic sector which is described by the polar coordinates (r, θ) . The total number of points on the grids is 250×250 points, as mentioned in Sec. III A. Therefore, for the j th grid (r_j, θ_j) , the Husimi function is given by $H_k^j = H_k(r_j, \theta_j)$. Then, the information entropy can be numerically evaluated as

$$I_k = \sum_j I_k^j = - \sum_j S_j H_k^j \ln(H_k^j),$$

where $S_j = r_j \Delta r \Delta \theta$ is the area of the j th grid. Here, $\Delta r = r_{j+1} - r_j$ and $\Delta \theta = \theta_{j+1} - \theta_j$. Also, H_k^j are normalized such that $\sum_j S_j H_k^j = 1$. Finally, we numerically compute the localization measure as follows:

$$A_k = \frac{\exp(I_k)}{\sum_j S_j}.$$

In what follows, we will show that the localization measure probability distribution $P(A)$ is in good agreement with the

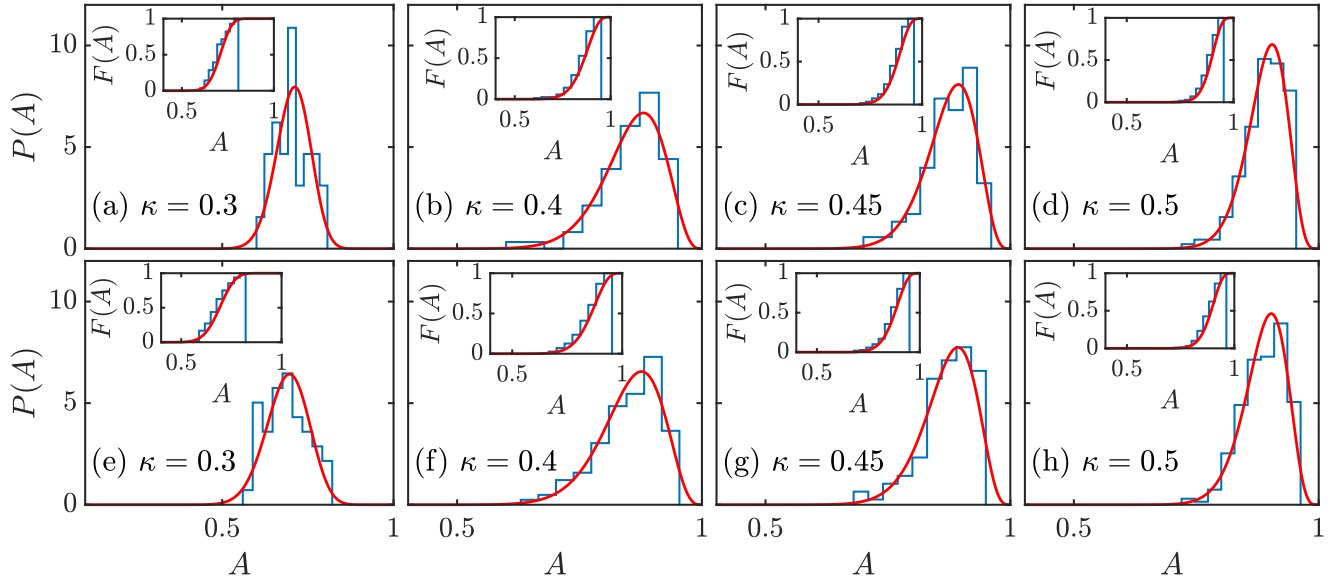


FIG. 9. First row [panels (a–d)]: Distribution $P(A)$ of the localization measure A for different values of κ with $N = 40$. The values of shape parameters (a, b) of the fitted β distribution from panel (a) to panel (d) are given by (58.18, 24.18), (26.51, 4.47), (35.45, 5.09), (50.21, 6.17). Second row [panels (e–h)]: Distribution $P(A)$ for several κ with $N = 48$. The inset in each panel corresponding to the cumulative distribution. The shape parameters (a, b) of the fitted β distribution are given by [panels (e) and (f)]: (38.25, 17.25), (26.09, 4.54), (34.84, 4.84), (49.71, 5.69). The red solid line in the main panels and insets are the β distribution and its cumulative distribution, respectively. The chaotic eigenstates that used in our calculation are identified by $M_k \geq M_t = 0.5$. The other parameters are: $\omega = \omega_0 = 1$. All quantities are dimensionless.

so-called β distribution,

$$P(A) = C_A A^{a-1} (1-A)^{b-1}, \quad (28)$$

where a and b are the two positive shape parameters, C_A is the normalization constant, which can be obtained from the normalization condition $\int_0^1 dA P(A) \equiv 1$, i.e., $C_A = \mathcal{B}^{-1}(a, b)$ with $\mathcal{B}(a, b) = \int_0^1 u^{a-1} (1-u)^{b-1} du$ is the β function. To further demonstrate the agreement between the probability distribution of A and the β distribution, we also consider the cumulative distribution defined as

$$F(A) = \int_0^A P(y) dy, \quad (29)$$

where $P(y)$ is the probability density function of A .

Figure 9 plots the localization measure probability distribution $P(A)$ for different coupling parameters κ with $N = 40$ (first row) and $N = 48$ (second row). The distributions $P(A)$ and $F(A)$ can be compared with the β distribution indicated by the red solid lines. From these results we make several observations: (i) Irrespective of the system size, since the degree of chaos of the system increases with an increase in κ , the larger is the value of κ , the better is the agreement between the β distribution and $P(A)$. (ii) For the cases which are well fitted by the β distribution, increasing κ leads to the decrease in the width of $P(A)$ and the peak value of $P(A)$ tends to 1, regardless of the system size. This reflects the fact that the degree of the delocalization of the chaotic eigenstates is increased as κ increases. (iii) The agreement between $P(A)$ and β distribution can be improved by increasing the system size. (iv) Because the regularity of the system increases with decreasing κ , there is an obvious deviation between $P(A)$ and β distribution at smaller κ , irrespective of the system size.

These features of $P(A)$ are qualitatively similar to the ones in billiards [43,44]. However, different from the billiards where the maximum value of A is given by 0.7, in our system we have $A_{\max} = 0.96$. The underlying reason of this deviation in the maximum value of localization measure calls for further investigation. Nevertheless, we believe that, in general, the localization measure probability distribution $P(A)$ is well described by the β distribution. A very interesting topic for further study concerns the theoretical understanding of the probability distribution $P(A)$.

To better understand the properties of localization in chaotic eigenstates, in the following, we focus on the relationship between the averaged localization measure, denoted by $\langle A \rangle$, and the level repulsion exponent.

B. The level repulsion exponent and $\langle A \rangle$ of the chaotic eigenstates

As one of the remarkable features of quantum chaos, level repulsion is usually used to define the quantum chaos. It is known that there is no level repulsion in integrable systems and the energy levels of them are uncorrelated, so the distribution $P(s)$ of the spacings, s , between neighboring energy levels is given by the Poissonian distribution [1],

$$P_P(s) = e^{-s}. \quad (30)$$

In contrast, in the fully chaotic systems the eigenvalues are correlated and exhibit a strong level repulsion. According to the random matrix theory, the level spacing distribution in those systems is given by the Wigner-Dyson distribution [1,2]. Depending on the symmetries in the system, the Wigner-Dyson distribution can be expressed in different forms. For the

systems with time reversal symmetry, which are represented by a Gaussian orthogonal ensemble, the Wigner-Dyson distribution is given as

$$P_W(s) = \frac{\pi s}{2} \exp\left(-\frac{\pi s^2}{4}\right). \quad (31)$$

Full chaos is an exception, a generic system usually exhibits a structured phase space which has both regular and chaotic regions. The level spacing distribution in those mixed-type Hamiltonian systems was explored in several works and has been found that it can be very well described by the so-call Berry-Robnik-Brody (BRB) distribution [39,93–95]. It has also been found that the level spacing distribution of the localized chaotic eigenlevels follows the well-known Brody distribution defined as [96,97]

$$P_B(s) = (\beta + 1)\zeta_\beta s^\beta \exp(-\zeta_\beta s^{\beta+1}), \quad (32)$$

where by using the required normalization and unfolding conditions, $\int_0^\infty P_B(s) ds \equiv 1$ and $\int_0^\infty s P_B(s) ds = 1$, one can find the factor ζ_β in the following form:

$$\zeta_\beta = \left[\Gamma\left(\frac{\beta + 2}{\beta + 1}\right) \right]^{\beta+1}, \quad (33)$$

with $\Gamma(x)$ being the γ function. The parameter β , which characterizes the signatures of the level spacing distribution as $s \rightarrow 0$, namely, $P_B(s \rightarrow 0) \propto s^\beta$, is the level repulsion exponent and varies from 0 to 1. For $\beta = 0$, we have $P_B(s) = P_P(s)$, indicating the maximal localization in chaotic eigenstates, while $\beta = 1$ leads to $P_B(s) = P_W(s)$, meaning the maximal extendedness in chaotic eigenstates. Therefore, a value of $\beta \in [0, 1]$ obtained from a concerted level spacing distribution tells us what the degree of localization as reflected in chaotic eigenlevels is. In our study, to get the level repulsion exponent β , we employ the following identity [94]:

$$\begin{aligned} \mathcal{L}_c^B(s) &= (\beta + 1) \ln s + \ln \zeta_\beta, \\ \mathcal{L}_c^B(s) &= \ln\{\ln[1 - G(s)]^{-1}\}. \end{aligned} \quad (34)$$

Here, $G(s) = \int_0^s P_B(s') ds'$ is the cumulative distribution of the Brody distribution. Hence, the level repulsion exponent β can be easily obtained through a simple linear fit of the left-hand side of Eq. (34) in the logarithmic scale of the level spacings s .

An example is demonstrated in Fig. 10. We can see that the numerical data are well fitted by Eq. (34), and the level spacing distribution of the chaotic eigenstates is in good agreement with the Brody distribution (see the inset of Fig. 10). We would like to point out that there exist several different distributions that can be interpolated between the Poisson and Wigner distributions, such as the Izrailev distribution [26]. The reasons we choose Brody distribution in our study are two. First, the Brody distribution has a simpler formula than the others, therefore it is easier to calculate the level repulsion exponent. Second and important, recent numerical results have shown that the Brody distribution is better in describing the real data [39,40,98].

By utilizing Eq. (34), the level repulsion exponent β of chaotic eigenstates has been calculated for different system sizes with $\kappa \in (0.3, 0.55)$ and $\epsilon \in (0.44, 0.95)$. The variation of β with the averaged localization measure $\langle A \rangle$ for different system sizes are depicted in Fig. 11. We see an obvious linear

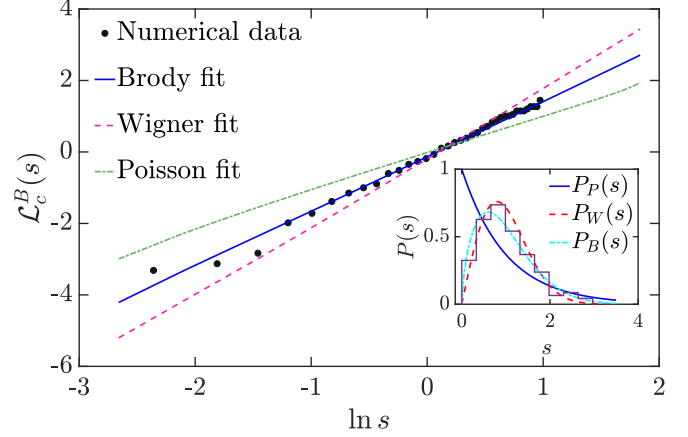


FIG. 10. \mathcal{L}_c^B in Eq. (34) as a function of $\ln s$ for unfolded eigenlevels of the chaotic eigenstates with $\kappa = 0.48$ and $N = 48$. The linear fit (blue solid line) of the numerical data determines the value of the level repulsion exponent in Brody distribution $\beta = 0.5936$. The level spacing distribution and its fitted Brody distribution are plotted in the inset. The employed chaotic eigenstates are identified by $M_k \geq M_l = 0.5$. The other parameters are: $\omega = \omega_0 = 1$. All quantities are dimensionless.

relationship between β and $\langle A \rangle$, regardless of the system size. Our results show that for the quantum many-body system with classical counterpart described by the smooth Hamiltonian, the proportionality between $\langle A \rangle$ and β still holds, as observed and discussed in quantum kicked rotator [99] and different billiards [42–44]. Therefore, we believe that this linear relationship is one of the universal features of the chaotic eigenstates.

The linear behavior exhibited by β with respect to $\langle A \rangle$ can be intuitively explained as follows. One consequence of the localization of chaotic eigenstates is the reduction of the correlations between eigenlevels. Hence, the increase in the

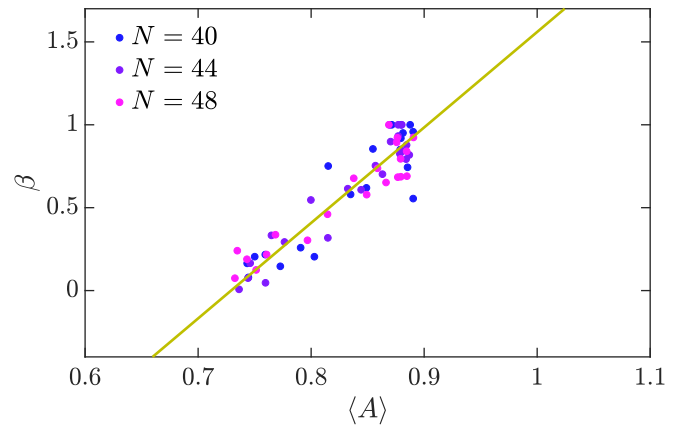


FIG. 11. Level repulsion exponent β as a function of the averaged localization measure $\langle A \rangle$ for different systems sizes with $\kappa \in [0.3, 0.55]$ and $\epsilon \in (0.44, 0.95)$. The linear fit line (solid line) is given by $y = 5.76x - 4.2$. The chaotic eigenstates that are employed in our calculation are the states defined by $M_k \geq M_l = 0.5$. The other parameters are: $\omega = \omega_0 = 1$. The axes in the figure are dimensionless.

strength of localization (decreasing A) leads to the chaotic eigenlevels from being fully correlated with avoided crossings with $\beta = 1$, to a power-law-level repulsion with $0 < \beta < 1$. However, a better and deeper understanding of the relation between the localization and level repulsion requires a more general theoretical analysis. We leave this study as an open question for future work. Finally, we should point out that in contrast to the billiards, in which both $\langle A \rangle$ and β behave as a rational function with respect to α [cf. Eq. (17)], our numerical results (not shown here) indicate that $\langle A \rangle$ and β are independent of the value of α (in a relatively small α interval) in the Dicke model. However, to get deeper understanding of the relations between them, more works are still required.

V. CONCLUSIONS

In conclusion, aimed to explore the localization properties of the chaotic eigenstates and their spectral statistics in the smooth Hamiltonian, we have examined the properties of the localized chaotic eigenstates in Dicke model, in correspondence with its classical dynamics. As a paradigmatic spin-boson model, the Dicke model has been studied in several areas of physics. The classical counterpart of the Dicke model is described by a smooth Hamiltonian with two degrees of freedom.

The degree of localization in the chaotic eigenstates is determined by the parameter $\alpha = t_H/t_D$, defined as the ratio between the Heisenberg time t_H and the classical diffusion time t_D . After separating the chaotic eigenstates from the regular ones, we have shown that the localization measure A , which is defined in terms of the information entropy of the Husimi function, is linearly dependent on the participation number, indicating that they are equivalent, consistent with the results obtained in billiards. This result further confirms

that this is a general feature of the localization measure. We found that the localization measure probability distribution $P(A)$ is in good agreement with the so call β distribution and approaches the delta distribution as $\alpha \rightarrow \infty$. The same behaviors of $P(A)$ were also observed in different billiards. We also demonstrated that the level repulsion exponent of the chaotic eigenlevels behaves as a linear function with respect to the averaged localization measure $\langle A \rangle = \int dA A P(A)$, as observed also in the studies of billiards.

The above facts lead us to believe that our results hold also in other quantum systems, such as the hydrogen atom in strong magnetic field [100–104]. It is an interesting topic for future work to systematically explore the properties of the localized chaotic eigenstates in various time-independent quantum systems. Moreover, theoretically analyzing the nature of localization properties of chaotic eigenstates remains an open question, we will leave this study for future work.

We would also like to stress that, as an extension of the previous works in different billiards, our results in the present work help us to gain even more insights into the localization features of the chaotic eigenstates. Finally, the current progress in experimental technologies enables the realization of the Dicke model considered in this work, and therefore we expect that our studies can induce more experimental explorations in the localization properties of time-independent quantum systems.

ACKNOWLEDGMENTS

This work was supported by the Slovenian Research Agency (ARRS) under the Grants No. J1-9112 and No. P1-0306. Q.W. acknowledges support from the National Science Foundation of China under Grant No. 11805165, Zhejiang Provincial Nature Science Foundation under Grant No. LY20A050001.

-
- [1] F. Haake, *Quantum Signatures of Chaos* (Springer, Berlin, 1991).
 - [2] O. Bohigas, M. J. Giannoni, and C. Schmit, *Phys. Rev. Lett.* **52**, 1 (1984).
 - [3] H.-J. Stöckmann, *Quantum Chaos: An Introduction* (American Association of Physics Teachers, College Park, MD, 2000).
 - [4] S. Gnutzmann and A. Altland, *Phys. Rev. Lett.* **93**, 194101 (2004).
 - [5] S. Müller, S. Heusler, P. Braun, F. Haake, and A. Altland, *Phys. Rev. Lett.* **93**, 014103 (2004).
 - [6] M. Robnik, *Eur. Phys. J.: Spec. Top.* **225**, 959 (2016).
 - [7] A. Peres, *Phys. Rev. A* **30**, 1610 (1984).
 - [8] R. A. Jalabert and H. M. Pastawski, *Phys. Rev. Lett.* **86**, 2490 (2001).
 - [9] T. Gorin, T. Prosen, T. H. Seligman, and M. Žnidarič, *Phys. Rep.* **435**, 33 (2006).
 - [10] E. B. Rozenbaum, S. Ganeshan, and V. Galitski, *Phys. Rev. Lett.* **118**, 086801 (2017).
 - [11] I. García-Mata, M. Saraceno, R. A. Jalabert, A. J. Roncaglia, and D. A. Wisniacki, *Phys. Rev. Lett.* **121**, 210601 (2018).
 - [12] F. Borgonovi, F. Izrailev, L. Santos, and V. Zelevinsky, *Phys. Rep.* **626**, 1 (2016).
 - [13] C. T. West, T. Kottos, and T. Prosen, *Phys. Rev. Lett.* **104**, 054102 (2010).
 - [14] I. García-Mata, C. Pineda, and D. A. Wisniacki, *J. Phys. A: Math. Theor.* **47**, 115301 (2014).
 - [15] I. García-Mata, C. Pineda, and D. Wisniacki, *Phys. Rev. A* **86**, 022114 (2012).
 - [16] S. Mudute-Ndumbe and E.-M. Graefe, *arXiv:1912.09412*.
 - [17] P. Kos, M. Ljubotina, and T. Prosen, *Phys. Rev. X* **8**, 021062 (2018).
 - [18] B. Bertini, P. Kos, and T. Prosen, *Phys. Rev. Lett.* **121**, 264101 (2018).
 - [19] A. Chan, A. De Luca, and J. T. Chalker, *Phys. Rev. X* **8**, 041019 (2018).
 - [20] A. J. Friedman, A. Chan, A. De Luca, and J. T. Chalker, *Phys. Rev. Lett.* **123**, 210603 (2019).
 - [21] L. D'Alessio, Y. Kafri, A. Polkovnikov, and M. Rigol, *Adv. Phys.* **65**, 239 (2016).
 - [22] D. A. Abanin, E. Altman, I. Bloch, and M. Serbyn, *Rev. Mod. Phys.* **91**, 021001 (2019).

- [23] R. Blümel and U. Smilansky, *Phys. Rev. Lett.* **58**, 2531 (1987).
- [24] B. V. Chirikov, F. Izrailev, and D. Shepelyansky, *Sov. Scient. Rev. C* **2**, 209 (1981).
- [25] G. Casati, B. V. Chirikov, D. L. Shepelyansky, and I. Guarneri, *Phys. Rep.* **154**, 77 (1987).
- [26] F. M. Izrailev, *Phys. Rep.* **196**, 299 (1990).
- [27] S. Fishman, D. R. Grempel, and R. E. Prange, *Phys. Rev. Lett.* **49**, 509 (1982).
- [28] G. Casati, B. Chirikov, F. Izrailev, and J. Ford, in *Stochastic Behavior in Classical and Quantum Hamiltonian Systems* (Springer, Berlin, 1979), pp. 334–352.
- [29] M. Arndt, A. Buchleitner, R. N. Mantegna, and H. Walther, *Phys. Rev. Lett.* **67**, 2435 (1991).
- [30] F. L. Moore, J. C. Robinson, C. F. Bharucha, B. Sundaram, and M. G. Raizen, *Phys. Rev. Lett.* **75**, 4598 (1995).
- [31] T. Prosen, in *Proceedings of the International School of Physics “Enrico Fermi,” Course CXLI-II*, edited by G. Casati, I. Guarneri, and U. Smilyanski (IOS Press, Amsterdam, 2000).
- [32] E. B. Rozenbaum and V. Galitski, *Phys. Rev. B* **95**, 064303 (2017).
- [33] C. Rylands, E. B. Rozenbaum, V. Galitski, and R. Konik, *Phys. Rev. Lett.* **124**, 155302 (2020).
- [34] M. Fava, R. Fazio, and A. Russomanno, *Phys. Rev. B* **101**, 064302 (2020).
- [35] F. Borgonovi, G. Casati, and B. Li, *Phys. Rev. Lett.* **77**, 4744 (1996).
- [36] G. Casati, B. V. Chirikov, I. Guarneri, and F. M. Izrailev, *Phys. Rev. E* **48**, R1613 (1993).
- [37] K. M. Frahm and D. L. Shepelyansky, *Phys. Rev. Lett.* **78**, 1440 (1997).
- [38] A. M. Lane, R. G. Thomas, and E. P. Wigner, *Phys. Rev.* **98**, 693 (1955).
- [39] B. Batistić and M. Robnik, *J. Phys. A: Math. Theor.* **43**, 215101 (2010).
- [40] B. Batistić and M. Robnik, *Phys. Rev. E* **88**, 052913 (2013).
- [41] B. Batistić and M. Robnik, *J. Phys. A: Math. Theor.* **46**, 315102 (2013).
- [42] B. Batistić, Č. Lozej, and M. Robnik, *Nonlin. Phenom. Complex Syst.* **21**, 225 (2018).
- [43] B. Batistić, Č. Lozej, and M. Robnik, *Phys. Rev. E* **100**, 062208 (2019).
- [44] B. Batistic, Č. Lozej, and M. Robnik, *Nonlin. Phenom. Complex Syst.* **23**, 17 (2020).
- [45] R. H. Dicke, *Phys. Rev.* **93**, 99 (1954).
- [46] C. Emary and T. Brandes, *Phys. Rev. Lett.* **90**, 044101 (2003).
- [47] C. Emary and T. Brandes, *Phys. Rev. E* **67**, 066203 (2003).
- [48] T. Brandes, *Phys. Rev. E* **88**, 032133 (2013).
- [49] M. A. Bastarrachea-Magnani, S. Lerma-Hernández, and J. G. Hirsch, *Phys. Rev. A* **89**, 032101 (2014).
- [50] C. M. Lóbez and A. Relaño, *Phys. Rev. E* **94**, 012140 (2016).
- [51] P. Pérez-Fernández and A. Relaño, *Phys. Rev. E* **96**, 012121 (2017).
- [52] M. Kloc, P. Stránský, and P. Cejnar, *Phys. Rev. A* **98**, 013836 (2018).
- [53] S. Lerma-Hernández, J. Chávez-Carlos, M. A. Bastarrachea-Magnani, L. F. Santos, and J. G. Hirsch, *J. Phys. A: Math. Theor.* **51**, 475302 (2018).
- [54] S. Lerma-Hernández, D. Villaseñor, M. A. Bastarrachea-Magnani, E. J. Torres-Herrera, L. F. Santos, and J. G. Hirsch, *Phys. Rev. E* **100**, 012218 (2019).
- [55] A. Altland and F. Haake, *Phys. Rev. Lett.* **108**, 073601 (2012).
- [56] A. Altland and F. Haake, *New J. Phys.* **14**, 073011 (2012).
- [57] R. J. Lewis-Swan, A. Safavi-Naini, J. J. Bollinger, and A. M. Rey, *Nat. Commun.* **10**, 1581 (2019).
- [58] Y. Alavirad and A. Lavasani, *Phys. Rev. A* **99**, 043602 (2019).
- [59] G. M. Andolina, M. Keck, A. Mari, V. Giovannetti, and M. Polini, *Phys. Rev. B* **99**, 205437 (2019).
- [60] M. de Aguiar, K. Furuya, C. Lewenkopf, and M. Nemes, *Ann. Phys. Phys.* **216**, 291 (1992).
- [61] K. Furuya, M. C. Nemes, and G. Q. Pellegrino, *Phys. Rev. Lett.* **80**, 5524 (1998).
- [62] M. A. Bastarrachea-Magnani, B. López-del-Carpio, J. Chávez-Carlos, S. Lerma-Hernández, and J. G. Hirsch, *Phys. Rev. E* **93**, 022215 (2016).
- [63] M. A. Bastarrachea-Magnani, B. L. del Carpio, J. Chávez-Carlos, S. Lerma-Hernández, and J. G. Hirsch, *Phys. Scr.* **92**, 054003 (2017).
- [64] J. Chávez-Carlos, M. A. Bastarrachea-Magnani, S. Lerma-Hernández, and J. G. Hirsch, *Phys. Rev. E* **94**, 022209 (2016).
- [65] J. Chávez-Carlos, B. López-del-Carpio, M. A. Bastarrachea-Magnani, P. Stránský, S. Lerma-Hernández, L. F. Santos, and J. G. Hirsch, *Phys. Rev. Lett.* **122**, 024101 (2019).
- [66] K. Baumann, C. Guerlin, F. Brennecke, and T. Esslinger, *Nature* **464**, 1301 (2010).
- [67] M. P. Baden, K. J. Arnold, A. L. Grimsmo, S. Parkins, and M. D. Barrett, *Phys. Rev. Lett.* **113**, 020408 (2014).
- [68] Z. Zhang, C. H. Lee, R. Kumar, K. J. Arnold, S. J. Masson, A. L. Grimsmo, A. S. Parkins, and M. D. Barrett, *Phys. Rev. A* **97**, 043858 (2018).
- [69] A. Safavi-Naini, R. J. Lewis-Swan, J. G. Bohnet, M. Gärtner, K. A. Gilmore, J. E. Jordan, J. Cohn, J. K. Freericks, A. M. Rey, and J. J. Bollinger, *Phys. Rev. Lett.* **121**, 040503 (2018).
- [70] V. Oganesyan and D. A. Huse, *Phys. Rev. B* **75**, 155111 (2007).
- [71] Y. Y. Atas, E. Bogomolny, O. Giraud, and G. Roux, *Phys. Rev. Lett.* **110**, 084101 (2013).
- [72] N. Chavda, H. Deota, and V. Kota, *Phys. Lett. A* **378**, 3012 (2014).
- [73] W. Buijsman, V. Gritsev, and R. Sprik, *Phys. Rev. Lett.* **118**, 080601 (2017).
- [74] S. C. L. Srivastava, A. Lakshminarayan, S. Tomsovic, and A. Bäcker, *J. Phys. A: Math. Theor.* **52**, 025101 (2018).
- [75] A. Sarkar, M. Kothiyal, and S. Kumar, *Phys. Rev. E* **101**, 012216 (2020).
- [76] A. L. Corps and A. Relaño, *Phys. Rev. E* **101**, 022222 (2020).
- [77] W.-M. Zhang, D. H. Feng, and R. Gilmore, *Rev. Mod. Phys.* **62**, 867 (1990).
- [78] A. Voros, in *Lecture Notes in Physics*, Vol. 93 (Springer, Berlin, 1979), pp. 326–333.
- [79] E. Wigner, *Phys. Rev.* **40**, 749 (1932).
- [80] K. Husimi, *Proc. Phys. Math. Soc. Jpn.* **22**, 264 (1940).
- [81] E. Romera, R. del Real, and M. Calixto, *Phys. Rev. A* **85**, 053831 (2012).
- [82] R. del Real, M. Calixto, and E. Romera, *Phys. Scr.* **T153**, 014016 (2013).
- [83] L. Bakemeier, A. Alvermann, and H. Fehske, *Phys. Rev. A* **88**, 043835 (2013).

- [84] K. Furuya, M. de Aguiar, C. Lewenkopf, and M. Nemes, *Ann. Phys.* **216**, 313 (1992).
- [85] M. B. Cibils, Y. Cuche, P. Leboeuf, and W. F. Wreszinski, *Phys. Rev. A* **46**, 4560 (1992).
- [86] D. Thouless, *Phys. Rep.* **13**, 93 (1974).
- [87] S. Hikami, *Prog. Theor. Phys* **76**, 1210 (1986).
- [88] B. Georgeot and D. L. Shepelyansky, *Phys. Rev. Lett.* **79**, 4365 (1997).
- [89] R. Berkovits and Y. Avishai, *Phys. Rev. Lett.* **80**, 568 (1998).
- [90] V. V. Flambaum and F. M. Izrailev, *Phys. Rev. E* **64**, 036220 (2001).
- [91] I. García-Mata, A. J. Roncaglia, and D. A. Wisniacki, *Phys. Rev. E* **91**, 010902(R) (2015).
- [92] O. Giraud and I. García-Mata, *Phys. Rev. E* **94**, 012122 (2016).
- [93] M. V. Berry and M. Robnik, *J. Phys. A: Math. Gen.* **17**, 2413 (1984).
- [94] T. Prosen and M. Robnik, *J. Phys. A: Math. Gen.* **27**, 8059 (1994).
- [95] T. Prosen and M. Robnik, *J. Phys. A: Math. Gen.* **32**, 1863 (1999).
- [96] T. A. Brody, *Lettere al Nuovo Cimento (1971–1985)* **7**, 482 (1973).
- [97] T. A. Brody, J. Flores, J. B. French, P. A. Mello, A. Pandey, and S. S. M. Wong, *Rev. Mod. Phys.* **53**, 385 (1981).
- [98] T. Manos and M. Robnik, *Phys. Rev. E* **87**, 062905 (2013).
- [99] T. Manos and M. Robnik, *Phys. Rev. E* **91**, 042904 (2015).
- [100] M. Robnik, *J. Phys. A: Math. Gen.* **14**, 3195 (1981).
- [101] M. Robnik, *J. Phys. Colloques* **43**, C2 (1982).
- [102] H. Hasegawa, M. Robnik, and G. Wunner, *Prog. Theor. Phys. Suppl.* **98**, 198 (1989).
- [103] H. Friedrich and H. Wintgen, *Phys. Rep.* **183**, 37 (1989).
- [104] H. Ruder, G. Wunner, H. Herold, and F. Geyer, *Atoms in Strong Magnetic Fields: Quantum Mechanical Treatment and Applications in Astrophysics and Quantum Chaos* (Springer Science & Business Media, Berlin, 2012).